

Layer-by-layer assembled enzyme multilayers with adjustable memory performance and low power consumption *via* molecular-level control†Hyunhee Baek,^{‡,a} Chanwoo Lee,^{‡,b} Jeongju Park,^{‡,b} Younghoon Kim,^a Bonkee Koo,^a Hyunjung Shin,^b Dayang Wang^c and Jinhan Cho^{*a}

Received 29th November 2011, Accepted 4th January 2012

DOI: 10.1039/c2jm16231h

Electrochemical properties of enzymes are of fundamental and practical importance in bio-electrochemical applications. These redox properties, which can cause the reversible changes in the current according to their redox reactions in solution, often depend on the chemical activity of transition metal ions as cofactors within the active sites of enzymes. Here, we demonstrate that the reversible resistance changes in enzyme-based multilayer films can be caused by the externally applied voltage as a result of charge trap/release of haem Fe^{III}/Fe^{II} redox couples in dry form. It is also demonstrated that the electrically bistable switching properties of redox enzymes can be applied to nonvolatile memory devices requiring low power consumption. For this study, cationic poly(allylamine hydrochloride) (PAH) was alternately layer-by-layer assembled with anionic catalase enzyme onto Pt-coated substrates until the desired number of layers was deposited. A top electrode was deposited onto (PAH/catalase)_n multilayer films to complete device fabrication. When an external bias was applied to the devices, a switching phenomenon depending on the voltage polarity (*i.e.*, bipolar switching) was observed at low operating voltages (RESET at 1.8 V and SET voltage at -1.5 V), fast switching speed at the nanosecond level, and an ON/OFF current ratio of ~10². In the case of inserting insulating layers of about 2 nm thickness between adjacent catalase (CAT) layers, these devices exhibited the higher memory performance (ON/OFF current ratio of ~10⁶) and the lower power consumption than those of (PAH/CAT)₁₅ multilayer devices.

Introduction

Redox enzymes have attracted considerable attention in the bioelectronic field such as for sensor devices and biofuel cells because they regulate a variety of biochemical reactions with high specificity under mild conditions.¹⁻⁴ These biochemical reactions are mainly caused by the presence of redox active sites, mostly related to the efficient charge transport using mediated or direct electron transfer between redox proteins and electrodes in an electrolyte aqueous solution. For example, catalase (CAT), which is a common enzyme found in nearly all living organisms, has the haem Fe^{III}/Fe^{II} redox couples.^{5,6} Considering that these redox reactions are closely related to electron release (oxidation) and trapping (reduction), redox enzymes may have electrically

bistable properties which cause a reversible change in resistance according to the externally applied low voltage. This possibility is very significant because a variety of biomaterials demonstrating redox reactions can be employed as active materials for the resistive switching-based nonvolatile memory (RSNM)⁷⁻¹⁵ devices applicable to mobile electronics such as MP3 players, digital cameras, and mobile phones requiring low power consumption. Although enzyme-based memory devices have been reported by Katz and co-workers, their memory devices rely on the electrochemical reaction of redox enzymes in aqueous buffer solution.¹⁶

In this study, we demonstrate that the redox enzymes such as CAT can be used as resistive switching active materials for nonvolatile memory devices and that furthermore these film devices can display high memory performance with low power consumption *via* layer-by-layer (LbL)-based molecular-level manipulation. To date, a number of new organic and inorganic materials, such as metal nanoparticles, transition metal oxides, and conjugated molecules and polymers, have been deliberately synthesized to construct RSNM devices.⁷⁻¹⁵ However, the flexibility and feasibility of RSNM device construction and application have been limited by the chemical complexity of material synthesis and the processing difficulty. To address this issue, and

^aDepartment of Chemical and Biological Engineering, Korea University, Anam-dong, Seongbuk-gu, Seoul, 136-713, Korea. E-mail: jinhan71@korea.ac.kr; Fax: +82 2 926 6102; Tel: +82 2 3290 4852

^bSchool of Advanced Materials Engineering, Kookmin University, Jeongneung-dong, Seongbuk-gu, Seoul, 136-701, Korea

^cIan Wark Research Institute, University of South Australia, Adelaide, SA5095, Australia

† Electronic supplementary information (ESI) available. See DOI: 10.1039/c2jm16231h

‡ These authors equally contributed to this work.

furthermore exploit the nonvolatile memory behavior of redox enzymes, we employed the catalase (CAT) enzyme commonly found in living organisms, instead of synthesizing new materials.

For this investigation, the multilayer films composed of anionic CAT and cationic polyelectrolyte (PE) were prepared on Pt-coated substrates using the electrostatic LbL assembly method, which enables the preparation of films with controlled thickness, composition and functionality on substrates of different sizes and shapes.^{17–36} Our LbL deposition for the build-up of CAT-based multilayers followed the process suggested by the Caruso group.²³ It has been demonstrated that the LbL assembly method is effective for the preparation of various electronic devices. For example, it was reported that LbL multilayer films could be extended to a rectifying junction diode.^{21,22} Recently, the Advincula group reported that nanometre-scale charging in LbL films based on conjugated polymers can provide a write–read memory device using current-sensing atomic force microscopy.²⁰ More recently, the Pal group reported that the electrostatically assembled multilayers composed of CdSe quantum dots can display electrical bistability.²⁷ The importance of this work lies in the possibilities for various enzymes containing transition metal ions to be used as resistive switching active materials for nonvolatile memory devices in a dry form. Furthermore, another aim of our work was to use the LbL assembly method to significantly improve the memory performance and power consumption of LbL-assembled film devices by the additional insertion of insulating PEs with nanoscale-thickness. We believe that our approach can provide a basis for exploiting the memory function of redox enzymes and developing the RSNM devices with high memory performance and energy saving.

Experimental section

Preparation of multilayers

The concentration of CAT (from bovine liver, Aldrich) and poly(allylamine hydrochloride) (PAH) ($M_w = 70\,000$, Aldrich) solutions used for all the experiments was 1 mg mL^{-1} . The solution pH of CAT and PAH was adjusted to 9. In this case, CAT was used as an anionic component at pH 9, and on the other hand, PAH was used as a cationic component. Pt-coated Si substrates had an anionic surface by irradiating UV light. These substrates were first dipped for 10 min in the cationic PAH solution, washed twice by dipping in water for 1 min, and air-dried with a gentle stream of nitrogen. Anionic CAT was subsequently deposited onto the PAH-coated substrates by using the same adsorption, washing, and drying procedures as described above. This process was repeated until the desired number of layers was deposited. The resultant multilayer films were thermally dried at $150\text{ }^\circ\text{C}$ for 1 h under air conditions to remove the residual water within films.

Zeta-potential measurement

The zeta-potentials of catalase were measured using an electrophoretic light scattering spectrophotometer (ELS-8000) when the respective micelles were alternately adsorbed onto 600 nm diameter silica particles. (PAH/CAT)₂-coated silica particles were prepared as follows: 0.5 mL of PAH (1 mg mL^{-1} at pH 9)

was added to negatively charged 600 nm silica particles and, after 20 min, the excess catalase was removed by three repeated centrifugations ($7000g$, 5 min)/wash cycles. The CAT (1 mg mL^{-1} at pH 9) was then deposited onto the catalase-coated PS particles under the same conditions. The above process was repeated until 4 layers were deposited and then ζ -potentials of these colloids were measured with increasing pH from 0 to 4.

QCM measurements

A QCM device (QCM200, SRS) was used to investigate the mass of material deposited after each adsorption step. The resonance frequency of the QCM electrodes was *ca.* 5 MHz. The adsorbed mass of PAH and biomaterials, Δm , can be calculated from the change in QCM frequency, ΔF , according to the Sauerbrey equation: $\Delta F\text{ (Hz)} = -56.6 \times \Delta m_A$, where Δm_A is the mass change per quartz crystal unit area in $\mu\text{g cm}^{-2}$.

Fabrication of resistive switching memory devices

All the samples were prepared on Si substrates ($2\text{ cm} \times 2\text{ cm}$) with SiO_2 layers of about 100 nm thickness. A Ti layer of 20 nm thickness was then deposited on the substrates and the bottom electrode (Pt) was subsequently deposited using a DC-magnetron sputtering system. The (PAH/CAT)_n multilayer films were then formed on the Pt-coated Si substrates. The resultant multilayer films were thermally annealed at $150\text{ }^\circ\text{C}$ for 1 h under air conditions. After thermal annealing, top electrodes with 100 μm diameter were deposited onto the nanocomposite films. To investigate the resistive switching behavior of LbL multilayered devices, the current–voltage (I – V) curves were measured by a semiconductor parametric analyzer (SPA, Agilent 4155B) in the air environment. The pulsed voltage duration dependence of high and low current states was investigated using a semiconductor parametric analyzer (HP 4155B) and a pulse generator (Agilent 8110A). *Although Ag electrodes were used as a top electrode in these devices, a similar switching behavior was also observed from Au, Pt or tungsten top electrodes. This indicates that the Ag electrode itself has no significant effect on the resistive switching characteristics of LbL (PE/enzyme or haemoglobin)_n multilayers.* For measuring the resistive switching memory of devices, at least 50 samples were prepared and tested and the respective samples had a few hundreds of electrodes. We have checked the electrical switching properties from about 100 samples, and resultantly obtained the reasonable switching results with about 80% yield in laboratory environments.

Current sensing atomic force microscopy

Local current maps at the nanoscale level were measured using current sensing atomic force microscopy (CS-AFM) (e-sweep, SEIKO). For the CS-AFM measurement, a CS-AFM tip (*i.e.*, Pt tip) with a diameter of about 10 μm was used as a top electrode instead of Ag electrodes.

Results and discussion

CAT is negatively charged in a phosphate buffer solution (PBS) of pH 7.0 because the isoelectric point (pI) of CAT is approximately 5.6.²⁸ In our work, anionic CAT and a polycation with

a pK_a of 9, poly(allylamine hydrochloride) (PAH),²⁸ were alternately deposited onto quartz crystal microgravimetry (QCM) or ITO electrodes using the electrostatic LbL assembly method. This method was quantitatively assessed using QCM. A change in the QCM frequency ($-\Delta F$) or mass (Δm) clearly demonstrates the LbL growth of a PAH/CAT multilayer film (Fig. 1a). The deposition of each layer of PAH or CAT resulted in a $-\Delta F$ of 30 ± 2 or 83.8 ± 4 Hz, respectively, corresponding to a Δm of ~ 533.6 ng cm^{-2} or ~ 1480.6 ng cm^{-2} . In addition, the thickness of the PAH/CAT multilayers increased from approximately 18 nm to 52 nm as the number of bilayers increased (from 5 to 15 bilayers) (see ESI, Fig. S1†).

The bare ITO electrodes and the ITO electrodes coated with pure PE multilayer films composed of poly(allylamine hydrochloride) (PAH) and poly(4-styrene sulfonic acid) did not exhibit a noticeable redox current response in the range of potentials from -0.4 to 0.1 V (data not shown). In contrast, the CAT/PAH multilayer films exhibited a typical electrochemical redox behavior; an oxidation peak was present at ~ -0.1 V, and a reduction peak was present at ~ -0.25 V (Fig. 1b). These peaks were induced by the haem $\text{Fe}^{\text{III}}/\text{Fe}^{\text{II}}$ redox couples of the CATs in the films. Furthermore, these resulting films were dried at 150 °C for 1 h to completely remove the residual water from the films. As a result, the thickness of the PAH/CAT multilayer films decreased from 52 nm to approximately 49 nm because of the formation of a densely packed structure that was caused by the removal of the residual water (see ESI, Fig. S1†).

The biological redox activity of PAH/CAT multilayers was examined by monitoring their catalytic activity toward H_2O_2 . In this case, the inherent biological activity was significantly degraded after thermal drying (see ESI, Fig. S2†). However, these multilayers remained fairly active showing the typical redox reaction occurring from $\text{Fe}^{\text{III}}/\text{Fe}^{\text{II}}$ couples in PBS at pH 7.0 although the redox activity (*i.e.*, oxidation and reduction peak current) of the PAH/CAT multilayer films was altered after the thermal treatment (Fig. 1b). These results encouraged us to study the charge trap/release behavior of the haem $\text{Fe}^{\text{III}}/\text{Fe}^{\text{II}}$ couples of the CATs in the resulting multilayer films in their completely dry state.

Based on these results, we prepared nonvolatile memory devices based on $(\text{PAH}/\text{CAT})_n$ multilayers (Scheme 1). It should

be noted here that immobilized CAT-based films prepared by the LbL assembly method are very effective in elucidating their electrical switching properties due to the formation of relatively thick and densely packed films. Although we tried other chemical methods such as self-assembled monolayer (SAM) and simple spin-coating for single layer, the extremely thin layer (<10 nm thickness) allowing tunneling current caused a large amount of leakage current.

First, the electrical measurements of nonvolatile memory cells were performed with applied voltage in the air. In this case, Pt and Ag were used for the bottom and top electrodes, respectively. For the measurement of typical bipolar switching, voltage sweeps from -1.8 V to $+1.8$ V and back to -1.8 V were applied with the limited current compliance up to 100 mA. The high-current state (scan range over ± 1.8 V) formed after the initial electroforming stage (for a conductive path within multilayers) was suddenly converted to a low-current state at $+1.8$ V when the voltage polarity was reversely applied to the $(\text{PAH}/\text{CAT})_{n=5,10,15}$ multilayered devices. In addition, increasing the bilayer number (*i.e.*, increasing multilayer thickness) had a significant effect on lowering the current level, mainly the OFF current level because of the decrease of the electric field due to the increase of the film thickness (Fig. 2a). As a result, the ON/OFF current ratio of these devices was increased to a maximum of more than 10^2 . To evaluate device stability, cycling and retention time tests of 15 bilayered PAH/CAT film devices were carried out to determine their electrical stability in the ON and OFF states using a reading voltage of $+0.1$ V (Fig. 2b and c). In these cases, the ON and OFF states were kept continuously stable during the repeated cycling tests and a test period of 10^4 s in air. The multilayered devices displayed thermally stable memory reliability despite increasing the measurement temperature from 25 to 150 °C (Fig. 2c). When the current curves shown in Fig. 2c are replotted in $\log R_{\text{OFF}} - \text{Temp}$ (K) and in $\log R_{\text{ON}} - \text{Temp}$ (K), R_{ON} decreased linearly with increasing the measurement temperature, indicating that the conductive state is in the metallic state (*i.e.*, ohmic state) (Fig. 2d). On the other hand, the temperature dependence of R_{OFF} of the devices implies a semiconducting character (Fig. 2e). Recently, it was reported that proteins such as ferritin (with $\text{Fe}^{\text{III}}/\text{Fe}^{\text{II}}$ redox couples) are more conductive than apoferritin

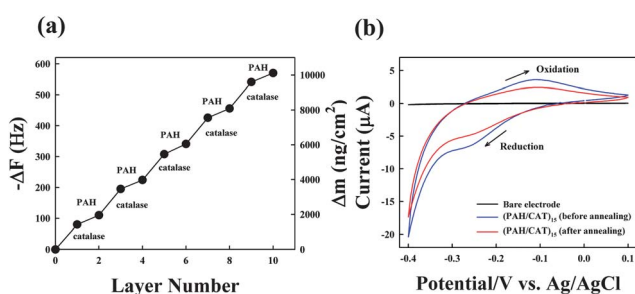
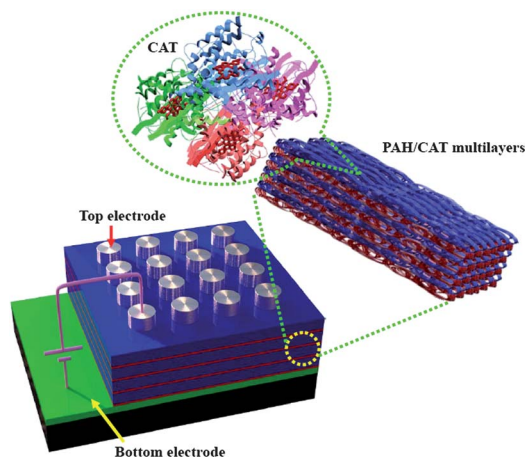


Fig. 1 (a) QCM data of PAH/CAT multilayers as a function of layer number. (b) Cyclic voltammogram of a $(\text{PAH}/\text{CAT})_{15}$ multilayer-coated electrode in pH 7.0 PBS with scan rate = 50 mV s^{-1} . These films were used without thermal annealing. The redox reaction results from the redox process of the $\text{Fe}^{\text{II}}/\text{Fe}^{\text{III}}$ couple in the haem prosthetic structure of CAT. In this case, it can be seen that in the potential region from -0.4 to 0.1 V, there is an oxidation peak at ~ -0.1 V and a reduction peak at ~ -0.25 V.



Scheme 1 Schematics for the set-up of PAH/CAT multilayer-based RSNM devices.

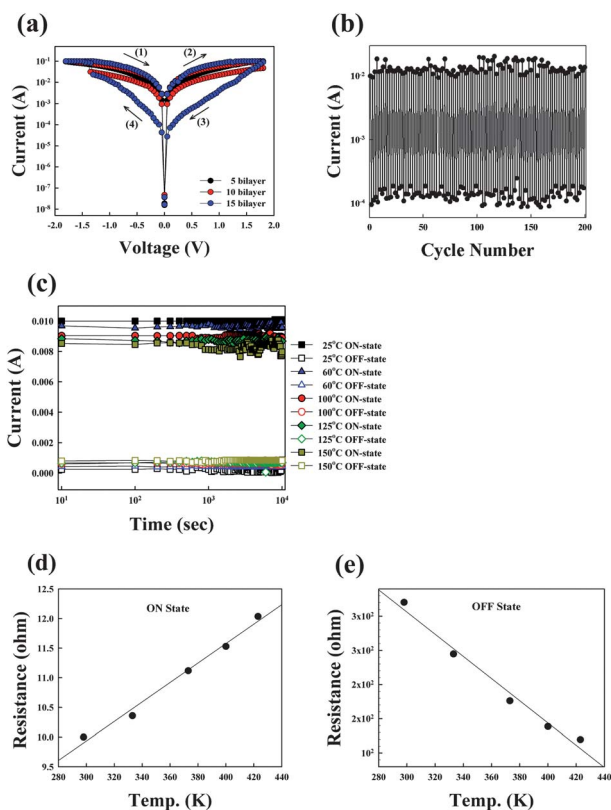


Fig. 2 (a) I - V curves of $(\text{PAH}/\text{CAT})_n$ multilayer devices with increasing bilayer number (n) from 5 to 15. (b) The cycling tests of a 15 bilayered device measured from the switching speed of 100 ns. (c) Retention time test of a 15 bilayered device measured at a reading voltage of 0.1 V with increasing the measurement temperature from 25 to 150 °C. Temperature dependence of (d) R_{ON} and (e) R_{OFF} of the device. R_{ON} decreases linearly with decreasing measurement temperature, indicating that the high conductive state is similar to the metallic state, and on the other hand, the temperature dependence of $\log R_{\text{OFF}}$ exhibits the semiconducting properties.

(without $\text{Fe}^{\text{III}}/\text{Fe}^{\text{II}}$ redox couples), showing the semiconducting behavior.³⁷ Furthermore, we have recently reported for the first time that the LbL multilayers based on proteins such as ferritin also can exhibit the nonvolatile memory properties in their dry form.³⁶

We also observed that CAT-based devices could be repeatedly operated at switching speeds ranging from 100 ns to 1 μs (Fig. 2b;

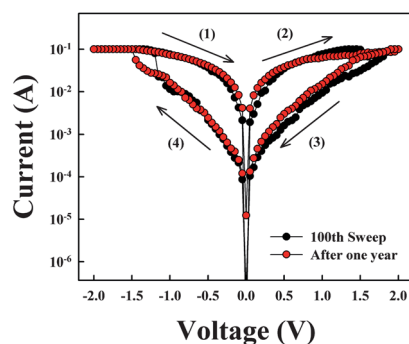


Fig. 3 I - V curves of $(\text{PAH}/\text{CAT})_{15}$ multilayers measured at 100th sweep and after one year in ambient air environments.

see ESI, Fig. S3†), and these reversible switching properties were maintained after one year (Fig. 3).

In the case of PAH/CAT multilayers dried at room temperature in a vacuum, the resulting device displayed an ON/OFF current ratio of greater than $\sim 10^2$, which was similar to that of the multilayers dried at 150 °C (Fig. 4a). In contrast, the conventional polyelectrolyte multilayers composed of cationic PAH and anionic poly(acrylic acid) (PAA) showed insulating characteristics without any switching memory (see ESI, Fig. S4†). These results imply that resistive switching properties of LbL multilayer devices exhibiting the good electrical stability and fast switching speed mainly originate from inherent CAT layers.

Recently, it was reported that solid electrolytes or transition metal oxides sandwiched between an electrochemically active Ag and an inert electrode showed resistive switching behavior because of an electrochemical redox reaction based on the high mobility of Ag ions.^{7,38–40} Although Ag electrodes were used as the top electrodes in our system, a similar switching behavior was also observed with electrochemically inert Au, Pt or tungsten (W) top electrodes (Fig. 4b).

In particular, $(\text{PAH}/\text{CAT})_{15}$ multilayers sandwiched between Pt (bottom) and tungsten tip (top) electrodes showed a relatively ON/OFF ratio above 10^2 using a reading voltage of +0.1 V. In this case, as a detachable tungsten tip electrode was used for physical contact with the CAT-based films instead of conventional vacuum deposition methods such as sputtering or evaporation for top electrode deposition, there was no metal ion diffusion into the films during physical contact with films or during device operation (by electrochemically inert tungsten). This observation indicates that the electroactive Ag electrode itself has no significant effect on the resistive switching characteristics of PAH/CAT multilayered devices.

The electrical properties of RSNM devices were also investigated with three different sizes of top electrodes (*i.e.*, 7, 100 and 500 μm diameter). In this case, there was no notable difference in

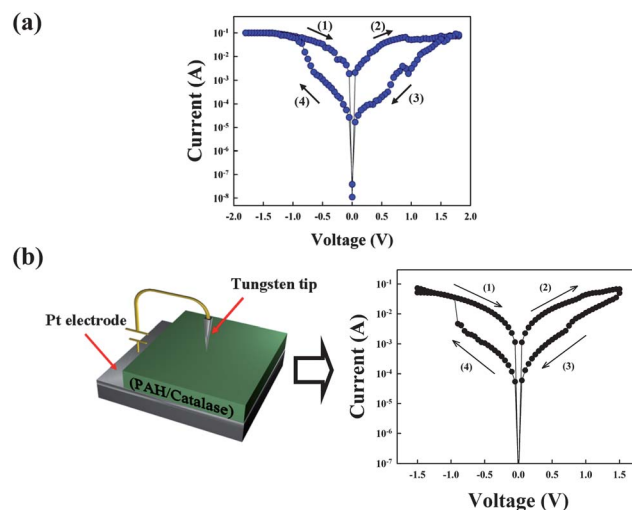


Fig. 4 (a) I - V curve of $(\text{PAH}/\text{CAT})_{15}$ multilayer devices. The multilayer film was sufficiently dried at room temperature in a vacuum before deposition of the top electrode. (b) I - V curves of $(\text{PAH}/\text{CAT})_{15}$ multilayers measured from the tungsten tip with a diameter of about 7 μm . The electrical measurements were operated at an applied voltage pulse with a 1 μs width in the air environment.

the RESET or SET current level between these devices. Although it was reported that the significant scaling down of the cell size from $100\ \mu\text{m} \times 100\ \mu\text{m}$ to $500\ \text{nm} \times 500\ \text{nm}$ could result in a decrease in RESET current of less than 1 order of magnitude,⁴¹ it was difficult to scale down the top electrodes to $\sim 100\ \text{nm}$ used in this study due to the limited capacity of the laboratory equipment.

To understand the conduction behavior of the CAT multilayers, the I - V characteristics of 15 bilayered films in the negative voltage sweep region were plotted and fitted on a log-log scale (Fig. 5a). The I - V relationship in the ON state clearly exhibits the ohmic conduction behavior with a slope of ~ 1.00 , which indicates the formation of conductive paths in the device during the SET process (*i.e.*, switching from the low current (OFF) to high current (ON) state). However, the conduction behavior in the OFF state is much more complicated. Fitting results for the high-resistance state indicate that the charge transport behavior agrees well with trap-controlled space charge limited conduction (SCLC),^{10,12} which consists of three different conductivity regions: the ohmic region ($I \propto V$) at low negative voltage, a transition region ($I \propto V^2$) from ohmic to SCLC transport, and the sharp current increase region. As a result, the different conduction behaviors in the ON and OFF states indicate that the ON/OFF switching of CAT-based memory devices is governed by the SCLC conduction and the localized conductive path.

The formation of conductive filamentary paths was also confirmed by current sensing atomic force microscopy (CS-AFM) characterizations (Fig. 5b and c).

In this case, a Pt tip was used as a top electrode instead of Ag electrode. The localized conductive paths were formed randomly after a V_{SET} of 5 V and disappeared from a V_{RESET} of $-5\ \text{V}$. That is, the formation and rupture of the randomly distributed

conductive paths were observed after “RESET” (*i.e.*, switching from the high current (ON) to low current (OFF) state) and “SET” processes (*i.e.*, switching from the low current (OFF) to high current (ON) state). This phenomenon suggests that the current density between the top and bottom electrodes is not uniform but concentrated in these localized conducting paths, which are turned on and off during switching. The rupture and formation of conductive filamentary path were formed from electron trap within and release from charge trap sites, respectively. It was reported that the wave character of the electron allows it to “mix” between the cofactors (charge trap sites) *via* proteins despite the insulating characteristics of the proteins.⁴²⁻⁴⁴ Considering that the internal structure of multilayers is not stratified but mixed structure due to a high degree of chain interdigitation between CAT and PAH layers, such interdigitated layers, facilitates electron-tunnelling across the organic layers (*i.e.*, CAT and PAH) between localization sites.

In addition, the V_{RESET} of 1.8 V and V_{SET} of $-1.5\ \text{V}$ shown in Fig. 2a were higher than those from the devices shown in CS-AFM. Although not completely understood, it is believed that the surface interfacial contamination on conducting AFM surfaces may provide an additional energy barrier for the increased voltage thresholds for set and reset. Furthermore, the possibility that the electric field exerted from the tip is non-uniform throughout the multilayer cannot be excluded because the conducting AFM tip can operate as an electrical point source. This non-uniform electric field can increase the applied voltages for resistive switching.

Although a variety of switching mechanisms (*i.e.*, memristor model,^{8,9} filamentary conduction model of a fuse-antifuse type⁴⁵ or charge transfer between active components with different energy levels⁴⁶) for resistive switching memory devices were reported by many other research groups, the memory effect with the high and low current states in our devices could be due to charge storage (high resistance) and release (low resistance) within charge trap sites.⁴⁷⁻⁴⁹ That is to say, the charge trap and release can cause the rupture and formation of conductive paths. In our system, the redox active sites within the multilayers can be used as charge-trap elements, which can considerably affect the switching mechanism. First, after initial electroforming, the negative voltage sweep of devices from $-1.8\ \text{V}$ to $0\ \text{V}$ releases the electrons from redox sites (*i.e.*, region (1) in Fig. 2a) and induces the high conductive state. This ON state is maintained until electrons are partially injected into redox sites (*i.e.*, (2) and trapped in redox sites by reversing the voltage polarity (*i.e.*, (2) \rightarrow (3)). However, after the reversal of the voltage polarity, the conductive paths for electron in CAT multilayers are broken down, resulting in a decrease in conductivity, corresponding to the RESET process (*i.e.*, switching from the high current (ON) to low current (OFF) state). The OFF state is maintained up to about $-1.5\ \text{V}$ (*i.e.*, region (4)). However, an increase in the external electric field for releasing the trapped electrons within redox sites (*i.e.*, region (4)) is thought to sharply increase the conductivity at the SET voltage (*i.e.*, $V_{\text{SET}} \approx -1.5\ \text{V}$), enhancing the tunneling probability (*i.e.*, the SET process) and resultantly forming conductive paths. Based on this switching mechanism, we also investigated the resistive switching properties of haemoglobin-based multilayer film devices (*i.e.*, (haemoglobin/PSS)₁₅). Although these devices exhibited a relatively low

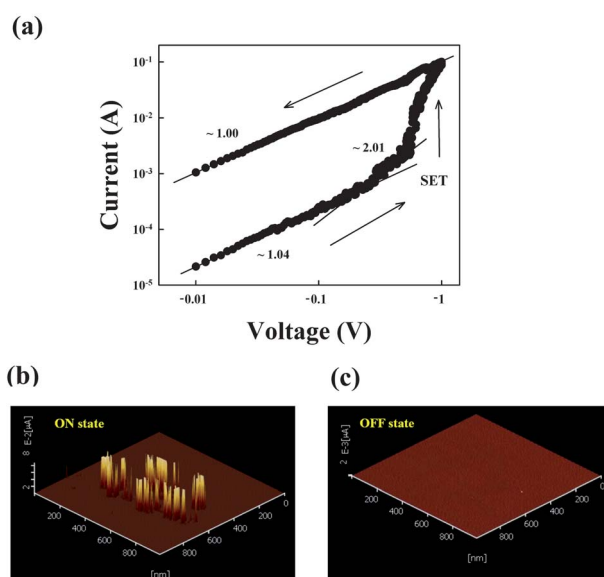


Fig. 5 (a) The linear fitting for the I - V curve of a 15 bilayered device in the log-log scale during the SET process in negative voltage sweep. CS-AFM images of (PAH/CAT)₅ multilayers in the (b) ON and (c) OFF state, respectively. An electrically inert Pt tip was used as a top electrode instead of Ag electrode. The localized conductive paths were formed randomly after V_{SET} and disappeared after the V_{RESET} process.

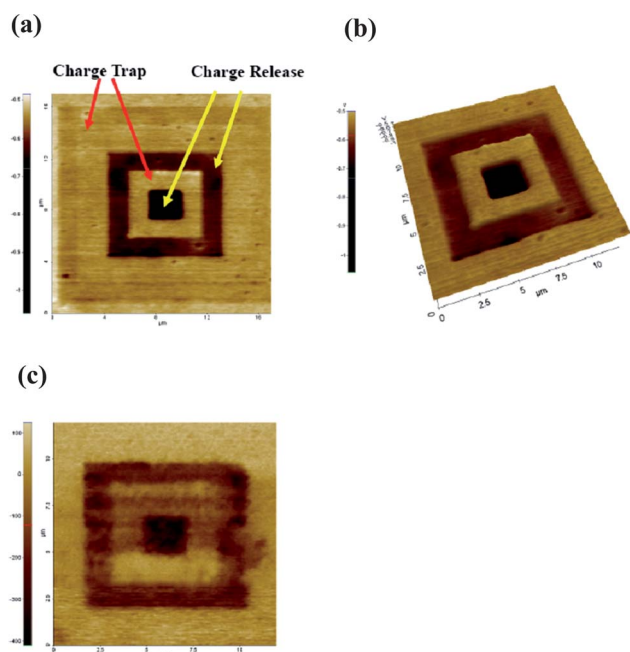


Fig. 6 (a) 2- and (b) 3-D scanning Kelvin probe force microscopy (KPFM) images of a PAH/CAT multilayered device for charge trap and release operation. (c) 2-D KPFM image of a single CAT layer onto the Pt-coated substrate for charge trap and release operation.

ON/OFF current ratio compared to that of CAT-based film devices, the haemoglobin-based film with $\text{Fe}^{\text{III}}/\text{Fe}^{\text{II}}$ redox couples evidently displayed the nonvolatile memory properties (Fig. S5†).

Furthermore, we confirmed the switching mechanism based on charge trap and release by Kelvin probe force microscopy (KPFM) which has been widely used to examine the changes in real-space imaging of the charge trap and release states. The charges stored within CAT could be detected from the change in surface potential when the tip (*i.e.*, Au-coated tip with 20 nm diameter) of the KPFM scans the surface of PAH/CAT multilayers (Fig. 6a and b). First, a $17 \times 17 \mu\text{m}^2$ area of multilayer films was scanned at 12 V for charge trap and then a $9 \times 9 \mu\text{m}^2$ area -12 V in a $9 \times 9 \mu\text{m}^2$ area for the charge release, respectively.

After that, the charge trap operation was successively performed by scanning a $5 \times 5 \mu\text{m}^2$ area with a $+12 \text{ V}$ and then -12 V bias in a $2 \times 2 \mu\text{m}^2$ area for charge release, again. As displayed in Fig. 6a, the yellow region indicates a charge trap

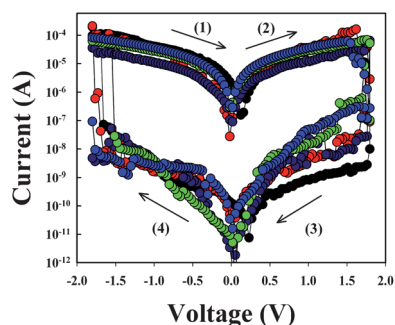


Fig. 7 I - V curves of $(\text{PAH}/\text{CAT}/\text{PAH}/\text{PAA})_{10}$ multilayer devices.

state and the dark region corresponds to the charge release state. This phenomenon was also confirmed by the KPFM image of a single CAT layer (Fig. 6c). Resultantly, these results evidently show that the nonvolatile devices composed of PAH/CAT multilayers are operated by the charge trap and release mechanism.

Based on these results, we have tried to significantly improve the memory performance of CAT multilayer devices by the structural design using LbL assembly. Our motivation was based on the possibilities that the further insertion of insulating layers of about 2 nm thickness between electrically active CAT layers could effectively screen the leakage current in ON and OFF current states, and resultantly induce the low level of power consumption. For this investigation, $(\text{PAH}/\text{CAT}/\text{PAH}/\text{PAA})_{10}$ multilayers were used instead of $(\text{PAH}/\text{CAT})_{15}$ multilayers (Fig. 7). These films were thermally annealed at $150 \text{ }^\circ\text{C}$ to completely remove the residual water within films. In this case, the $(\text{PAH}/\text{CAT}/\text{PAH}/\text{PAA})_{10}$ multilayer device exhibited the higher ON/OFF current ratio (10^5 to 10^6) and the lower current level (an ON current level of 10^{-5} A and an OFF current of 10^{-11} A at a reading voltage of -0.1 V) than those (an ON/OFF current ratio $\sim 10^2$, an ON current level of 10^{-2} and an OFF current level of 10^{-4} A at a reading voltage of -0.1 V) of the $(\text{PAH}/\text{CAT})_{15}$ multilayer device. On the other hand, operating voltages of these devices were not significantly increased compared to those of PAH/CAT multilayered devices. That is to say, the charge carriers (*i.e.*, electrons) captured in the CAT layers for the device containing CAT layers are sufficient to generate enough internal field to form the conducting filamentary paths across the inserted insulating layers with the decreased leakage current flow although the PAH/PAA film devices without CAT layers do not have the memory effect. This molecular-level control over device architecture *via* the use of the LbL assembly approach makes it possible to access the thickness regime and modulate the electrical properties simply not possible by conventional processing techniques.

Conclusions

We have demonstrated that immobilized enzymes in a dry state have unique electrical switching behaviors that can be used to create nonvolatile memory under applied voltages. These phenomena were found to be mainly caused by the charge trap/release of the haem $\text{Fe}^{\text{III}}/\text{Fe}^{\text{II}}$ redox couples within CAT. In addition, redox enzyme films were successfully applied to RSNM devices. Furthermore, it was also demonstrated that the molecular level control over structural design could significantly enhance the memory performance and energy saving of RSNM devices. Our approach—namely, using the redox active sites of biomaterials such as enzymes instead of synthetic inorganic and organic materials—will substantially widen the range of available materials for nonvolatile memory devices; various redox proteins extracted from living tissues, such as from the liver (for catalase), blood (for haemoglobin) and muscle (for myoglobin), will probably be used to fabricate electronic devices under non-liquid and non-physiological conditions. We believe that our approach can provide a basis for preparing the nonvolatile memory devices with adjustable memory performance and exploiting the novel resistive switching materials.

Acknowledgements

This work was supported by the National Research Foundation (NRF) grant funded by the Korea government (MEST) (2010-0029106; 2010-0027751; 2007-0057024), and ERC Program of KOSEF grant funded by the Korea government (MEST) (R11-2005-048-00000-0).

Notes and references

- 1 I. Willner, *Science*, 2002, **298**, 2407.
- 2 I. Willner and E. Katz, *Angew. Chem., Int. Ed.*, 2000, **39**, 1180–1218.
- 3 W. Jin, X. Shi and F. Caruso, *J. Am. Chem. Soc.*, 2001, **123**, 8121–8122.
- 4 V. L. Davidson, *Acc. Chem. Res.*, 2008, **41**, 730–738.
- 5 J. F. Rusling, *Acc. Chem. Res.*, 1998, **31**, 363–369.
- 6 Z. Zhang, S. Chouchane, R. S. Magliozzo and J. F. Rusling, *Anal. Chem.*, 2002, **74**, 163–170.
- 7 R. Waser and M. Aono, *Nat. Mater.*, 2007, **6**, 833–840.
- 8 D. V. Strukov, G. S. Snider, D. R. Stewart and R. S. Williams, *Nature*, 2008, **453**, 80–83.
- 9 J. J. Yang, M. D. Pickett, X. Li, D. A. A. Ohlberg, D. R. Stewart and R. S. Williams, *Nat. Nanotechnol.*, 2008, **3**, 429–433.
- 10 M. A. Lampert and P. Mark, *Current Injection in Solids*, Academic, New York, 1970.
- 11 J. C. Scott and L. D. Bozano, *Adv. Mater.*, 2007, **19**, 1452–1463.
- 12 R. T. Weitz, A. Walter, R. Engl, R. Sezi and C. Dehm, *Nano Lett.*, 2006, **6**, 2810–2813.
- 13 D. I. Son, T. W. Kim, J. H. Shim, J. H. Jung, D. U. Lee, J. M. Lee, W. I. Park and W. K. Choi, *Nano Lett.*, 2010, **10**, 2441–2447.
- 14 J.-G. Park, W.-S. Nam, S.-H. Seo, Y.-G. Kim, Y.-H. Oh, G.-S. Lee and U.-G. Paik, *Nano Lett.*, 2009, **9**, 1713–1719.
- 15 Y. Ji, B. Cho, S. Song, T.-W. Kim, M. Choe, Y.-H. Kahng and T. Lee, *Adv. Mater.*, 2010, **22**, 3071–3075.
- 16 (a) E. Katz and V. Privman, *Chem. Soc. Rev.*, 2010, **39**, 1835–1857; (b) M. Pita, G. Strack, K. MacVittie, J. Zhou and E. Katz, *J. Phys. Chem. B*, 2009, **113**, 16071–16076.
- 17 G. Decher, *Science*, 1997, **277**, 1232–1237.
- 18 F. Caruso, R. A. Caruso and H. Möwald, *Science*, 1998, **282**, 1111.
- 19 P. Podsiadlo, A. K. Kaushik, E. M. Arruda, A. M. Waas, B. S. Shim, J. Xu, H. Nandivada, B. G. Pumplun, J. Lahann, A. Ramamoorthy and N. A. Kotov, *Science*, 2007, **318**, 80–83.
- 20 G. Jiang, A. Baba and R. Advincula, *Langmuir*, 2007, **23**, 817–825.
- 21 T. Cassagneau, T. E. Mallouk and J. H. Fendler, *J. Am. Chem. Soc.*, 1998, **120**, 7848–7859.
- 22 D. M. Kaschak, J. T. Lean, C. C. Waraksa, G. B. Saupe, H. Usami and T. E. Mallouk, *Langmuir*, 2001, **105**, 8762–8769.
- 23 A. Yu and F. Caruso, *Anal. Chem.*, 2003, **75**, 3031–3037.
- 24 J. Lee, J. Cho, C. Lee, I. Kim, J. Park, Y. M. Kim, H. Shin, J. Lee and F. Caruso, *Nat. Nanotechnol.*, 2007, **2**, 790–795.
- 25 B. Lee, Y. Kim, S. Lee, Y. S. Kim, D. Wang and J. Cho, *Angew. Chem., Int. Ed.*, 2010, **49**, 359–363.
- 26 C. Lee, I. Kim, H. Shin, S. Kim and J. Cho, *Langmuir*, 2009, **25**, 11276–11281.
- 27 B. C. Das, S. K. Batabyal and A. J. Pal, *Adv. Mater.*, 2007, **19**, 4172–4176.
- 28 J. Park, I. Kim, H. Shin, Y. S. Kim, J. Bang, F. Caruso and J. Cho, *Adv. Mater.*, 2008, **20**, 1843–1848.
- 29 J. Choi and M. F. Rubner, *Macromolecules*, 2005, **38**, 116–124.
- 30 J. Schmitt, T. Gruenewald, G. Decher, P. S. Pershan, K. Kjaer and M. Loesche, *Macromolecules*, 1993, **26**, 7058–7063.
- 31 M. Lösche, J. Schmitt, G. Decher, W. G. Bouwman and K. Kjaer, *Macromolecules*, 1998, **31**, 8893–8906.
- 32 M. Yoon, Y. Kim and J. Cho, *ACS Nano*, 2011, **5**, 5417–5426.
- 33 S. Kim, Y. Kim, Y. Ko and J. Cho, *J. Mater. Chem.*, 2011, **21**, 8008–8013.
- 34 Y. Kim, C. Lee, I. Shim, D. Wang and J. Cho, *Adv. Mater.*, 2010, **22**, 5140–5144.
- 35 S. Kim, J. Park and J. Cho, *Nanotechnology*, 2010, **21**, 375702.
- 36 Y. Ko, Y. Kim, H. Baek and J. Cho, *ACS Nano*, 2011, **5**, 9918–9926.
- 37 D. Xu, G. D. Watt, J. N. Harb and R. C. Davis, *Nano Lett.*, 2005, **5**, 571–577.
- 38 K. Terabe, T. Hasegawa, T. Nakayama and M. Aono, *Nature*, 2005, **433**, 47–50.
- 39 Y. C. Yang, F. Pan, Q. Liu, M. Liu and F. Zeng, *Nano Lett.*, 2009, **9**, 1636–1643.
- 40 K. Tsunoda, Y. Fukuzumi, J. R. Jameson, Z. Wang, P. B. Griffin and Y. Nishi, *Appl. Phys. Lett.*, 2007, **90**, 113501.
- 41 S.-E. Ahn, M.-J. Lee, Y. Park, B. S. Kang, C. B. Lee, K. H. Kim, S. Seo, D.-S. Suh, D.-C. Kim, J. Hur, W. Xianyu, G. Stefanovich, H. Yin, I.-K. Yoo, J.-H. Lee, J.-B. Park, I. G. Baek and B. H. Park, *Adv. Mater.*, 2008, **20**, 924–928.
- 42 D. S. Bendall, *Protein Electron Transfer*, BIOS Scientific Publishers, Oxford, 1996.
- 43 H. B. Bertini, S. J. Lippard and J. S. Valentine, *Bioinorganic Chemistry*, University Science Books, Mill Valley, 1994.
- 44 A. M. Kuznetsov and J. Ulstrup, *Electron Transfer in Chemistry and Biology: an Introduction to the Theory*, John Wiley & Sons, New York, 1998.
- 45 F. A. Chudnovskii, I. I. Odynets, A. I. Pergament and G. B. Stefanovich, *J. Solid State Chem.*, 1996, **122**, 95–99.
- 46 J. Ouyang, C.-W. Chu, C. R. Szmamda, L. Ma, Y. Yang, J. Ouyang, C.-W. Chu, C. R. Szmamda, L. Ma and Y. Yang, *Nat. Mater.*, 2004, **3**, 918–922.
- 47 J. G. Simmons and R. R. Verderber, *Proc. R. Soc. London, Ser. A*, 1967, **301**, 77–102.
- 48 T.-L. Choi, K.-H. Lee, W.-J. Joo, S. Lee, T.-W. Lee and M. Y. Chae, *J. Am. Chem. Soc.*, 2007, **129**, 9842–9843.
- 49 H. P. Wang, S. Pigeon, R. Izquierdo and R. Martel, *Appl. Phys. Lett.*, 2006, **89**, 183502.